Journal of Materials Chemistry C

RSC Publishing

PAPER

View Article Online
View Journal | View Issue

Cite this: *J. Mater. Chem. C*, 2013, **1**, 5694

Synthesis of donor–acceptor molecules based on isoxazolones for investigation of their nonlinear optical properties†

Di Jiang,[a] Zheng Xue,[a] Yongjun Li,*[b] Huibiao Liu[b] and Wensheng Yang*[a]

Received 26th June 2013
Accepted 18th July 2013

DOI: 10.1039/c3tc31228c

www.rsc.org/MaterialsC

A series of donor–acceptor molecules that incorporate *N*,*N*-dimethylaniline or carbazole as the common electron donor and 3-phenyl-5-isoxazolone as the electron acceptor moiety have been synthesized and their structural and optical properties and self-assembly behaviors were investigated. All these compounds showed the property of aggregation induced emission (AIE). These compounds with different donors and different conjugation could be self-assembled into different superstructures such as ribbon-like architectures, hollow nanospheres, multilayer plates or rhombic microplates by phase transfer methodology or solvent-vapor techniques. Furthermore, the nonlinear optical (NLO) properties of the four D–A molecules were studied by the *Z*-scan technique and all of these compounds exhibited third-order nonlinear absorption effects.

Introduction

Intramolecular charge-transfer (ICT) compounds often have an electron-donor (D) moiety and an electron-acceptor (A) moiety connected by a π-conjugated bridge.[1] Such D–A-substituted conjugated molecules usually have π-electron delocalization and are strongly polarized which could widely be used as second- or third-order NLO materials.[2,3] The molecular chemical structures such as the type of D–A moieties, the distance between the D–A moieties, and the symmetry of the molecules would have significant effects on their nonlinear properties.[4] Organic chemistry provides a large number of advantages in designing and synthesizing these molecular materials. In general, designing of suitable D or A moieties over an extensive range of different functional units could efficiently control NLO properties of the D–A molecules.[5] Thus, much academic and technological research attention has been focused on the design and synthesis of the D–A molecules with high nonlinearity. The self-assembly of ICT compounds[5–7] has attracted considerable attention in diverse material fields such as nonlinear optical (NLO) materials,[8–10] electrogenerated chemiluminescence materials,[11–13] fluorescence probes,[14–16] and organic solar cells[17–19] for their architectural flexibility, easy fabrication, ultra-fast response capacity, and high nonlinearity.[20,21]

3-Phenyl-5-isoxazolone is a powerful electron acceptor, which could exhibit high nonlinearities when linked to different electron-donating units. Alías *et al.*,[22] Hua *et al.*[23] and Gong *et al.*[24] have designed and synthesized different D–A molecules in which isoxazolone acted as the electron-acceptor and investigated their second-order nonlinear optical properties, but the third-order nonlinear optical responses of the D–A molecules with isoxazolone have received only scant attention.

Herein, we designed and synthesized four D–A molecules based on isoxazolone, in which the donor moieties consisted of the *N*,*N*-dimethylaniline and the carbazole units, while the isoxazolone acted as the acceptor. Meanwhile, their photophysical, morphological and third-order nonlinear optical properties were described. The D–A molecules **CLS**, **DSS** and **CSS** could be self-assembled into stable and well-ordered superstructures with different morphologies. In addition these D–A configurations displayed the electron delocalization which would contribute to the remarkable NLO properties.

Results and discussion

Synthesis and characterization

Four donor–acceptor-conjugated organic molecules were designed and synthesized in which isoxazolone acted as the electron-accepting moiety and *N*,*N*-dimethylaniline or carbazole was used as the electron-donating moiety. The chemical structures of the four compounds are shown in Scheme 1. All the compounds could be synthesized *via* Knoevenagel condensation from the corresponding aldehyde and isoxazolone in good yields. **DLS** was synthesized according to the literature.[25] The

[a]*State Key Laboratory for Supramolecular Structures and Materials, College of Chemistry, Jilin University, Changchun 130012, P. R. China. E-mail: wsyang@jlu.edu.cn; Fax: +86-431-85168186; Tel: +86-431-85168185*

[b]*CAS Key Laboratory of Organic Solids, Beijing National Laboratory for Molecular Science (BNLMS), Institute of Chemistry, Chinese Academy of Sciences, Beijing, P. R. China. E-mail: liyj@iccas.ac.cn; Fax: +86-10-82616576; Tel: +86-10-82615870*

† Electronic supplementary information (ESI) available. CCDC 947161–947163. For ESI and crystallographic data in CIF or other electronic format see DOI: 10.1039/c3tc31228c

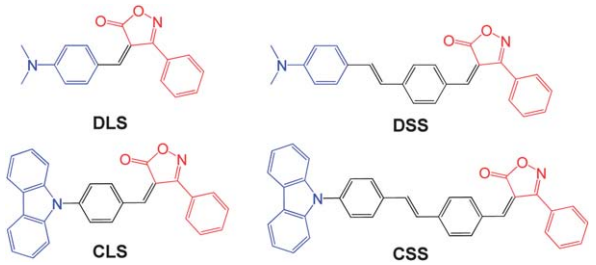

Scheme 1 Chemical structures of the donor–acceptor compounds.

other three were characterized by the ^{1}H, ^{13}C NMR spectra, mass spectra and the X-ray single-crystal determinations.

X-ray crystal structures

The single crystal of **DLS** suitable for X-ray determination was obtained by slow diffusion of methanol into CH_2Cl_2 solution. The **DLS** molecule was grown as plates, which could provide good quality crystal data. **DLS** shows a monoclinic *c*-centered *C* lattice with unit cell parameters of $a = 21.092(13)$ Å, $b = 6.521(3)$ Å, $c = 12.149(7)$ Å, and $\beta = 119.587(8)^\circ$; the space group is *Cc*. The detailed crystallographic data of the molecule are shown in Table S1.† The single-crystal structure and the packing diagram of **DLS** are shown in Fig. 1a and b. In **DLS**, the alkene between benzene ring and heterocyclic ring is in the *cis*-form. The heterocyclic ring plane and the benzene plane that are connected by alkene are almost in the same plane, which provides a good chance for electron transfer. From the packing diagram, we could learn that different pairs in the **DLS** molecule are held together by van der Waals forces. The benzene moieties of *N*,*N*-dimethylaniline exhibit a face-to-face π-stacking with an intermolecular distance of 3. 523 Å. CH–π interactions from the CH on the benzene ring to the benzene ring of other molecules and from the methylic hydrogen atom to the benzene ring exist in the crystal packing structure. Meanwhile, the hydrogen bonds between methylic hydrogen and carbonylic oxygen atoms, between hydrogen atom in alkene and carbonylic oxygen atom, and between the CH on the benzene ring and nitrogen atom in the heterocyclic ring also play important roles in the creation of the crystal packing structure.

The single crystal of **DSS** was obtained by slow evaporation of CH_2Cl_2 solution. The **DSS** molecule was grown as prisms, which could also provide good quality crystal data. **DSS** has a primitive orthorhombic crystal system with $a = 5.844(4)$ Å, $b = 7.720(5)$ Å, $c = 44.76(3)$ Å, and $\beta = 90^\circ$; the space group is $P2_12_12_1$. The alkene between two benzene rings is in the *trans*-form (Fig. 1c). However, the alkene between the benzene ring and heterocyclic ring is in the *cis*-form. The two benzene rings linked by the ethylenic linkage bond are almost in the same plane with a dihedral angle of 3.63°, which also suggests that an extended π-conjugated system exists in this part of the molecule.[26] The benzene ring moieties in *N*,*N*-dimethylaniline show π-stacking with an intermolecular distance of 3.724 Å (Fig. 1d). Meanwhile, numerous hydrogen bonds exist in the crystal packing structure between the methylic hydrogen atom in *N*,*N*-dimethylaniline and carbonylic oxygen atom, between the CH on the benzene and carbonylic oxygen atom, between the CH on the benzene and the oxygen in the heterocyclic ring. Besides, CH–π interactions from the CH on the benzene to the benzene ring of other molecule, from the methylic hydrogen atom to the benzene ring and alkenes also have influence on the structure of the packing.

Besides, a single crystal of **CSS** suitable for the determination was obtained by slow diffusion of hexane into CH_2Cl_2 solution. The **CSS** molecule was grown as rods, which could provide good quality crystal data. **CSS** indicates a monoclinic crystal system (Fig. 1e and f) with unit cell parameters of $a = 16.6077(15)$ Å, $b = 8.2169(8)$ Å, $c = 20.0522(2)$ Å, and $\beta = 109.011(11)^\circ$; the space group is $P2_1/n$. In **CSS**, the alkene between two benzene rings is in the *trans*-form. However, the alkene between benzene ring and heterocyclic ring is in the *cis*-form. The dihedral angle between two benzenes plane is 10.80°, which is larger than that in **DSS**. This might result from the distorting effect of the carbazole group in **CSS**. And the small dihedral angle also suggests the existence of an extended π-conjugated system in this part of the molecule. Meanwhile, the benzene moieties exhibit strong face-to-face π-stackings. CH–π interactions from the CH on the benzene to the carbazole group are also observed in the crystal packing.‡

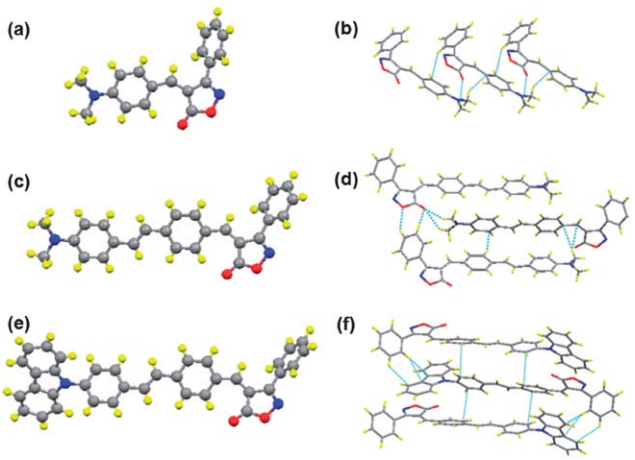

Fig. 1 The molecular structures and packing diagrams of **DLS** (a and b), **DSS** (c and d) and **CSS** (e and f).

‡ Crystal data for **DLS**: $C_{18}H_{16}N_2O_2$, $M = 292.33$, monoclinic, $a = 21.092(13)$ Å, $b = 6.521(3)$ Å, $c = 12.149(7)$ Å, $\alpha = 90^\circ$, $\beta = 119.587(8)^\circ$, $\gamma = 90^\circ$, $V = 1453.2(14)$ Å^3, $T = 173(2)$ K, space group *Cc*, $Z = 4$. The final R_1 values were 0.0539 ($I > 2\sigma(I)$). The final $wR(F^2)$ values were 0.1341 ($I > 2\sigma(I)$). The final R_1 values were 0.0556 (all data). The final $wR(F^2)$ values were 0.1356 (all data). Crystal data for **DSS**: $C_{26}H_{22}N_2O_2$, $M = 394.46$, orthorhombic, $a = 5.844(4)$ Å, $b = 7.720(5)$ Å, $c = 44.76(3)$ Å, $\alpha = 90^\circ$, $\beta = 90^\circ$, $\gamma = 90^\circ$, $V = 2019(2)$ Å^3, $T = 173(2)$ K, space group $P2_12_12_1$, $Z = 4$. The final R_1 values were 0.0851 ($I > 2\sigma(I)$). The final $wR(F^2)$ values were 0.1588 ($I > 2\sigma(I)$). The final R_1 values were 0.0942 (all data). The final $wR(F^2)$ values were 0.1635 (all data). Crystal data for **CSS**: $C_{36}H_{24}N_2O_2$, $M = 516.18$, monoclinic, $a = 16.6077(15)$ Å, $b = 8.2169(8)$ Å, $c = 20.0522(2)$ Å, $\alpha = 90^\circ$, $\beta = 109.011(11)^\circ$, $\gamma = 90^\circ$, $V = 2587.15$ Å^3, $T = 173(2)$ K, space group $P2_1/n$, $Z = 4$. The final R_1 values were 0.0528 ($I > 2\sigma(I)$). The final $wR(F^2)$ values were 0.1428 ($I > 2\sigma(I)$). The final R_1 values were 0.0718 (all data). The final $wR(F^2)$ values were 0.1649 (all data).

Photophysical properties

Fig. 2a shows the normalized optical absorption spectra of the four D–A molecules in CH_2Cl_2 solution (1×10^{-5} M). Two prominent absorption features are observed in the spectra of all the D–A molecules. The bands at lower wavelengths (~290 nm) would be associated with the π–π* transitions of the carbazole units in **CLS** and **CSS** molecules.[27] The bands at higher wavelengths (400–600 nm) could be assigned to intramolecular charge transfer (ICT) transitions in each D–A molecules.[28] The ICT absorption band of the D–A molecules would red shift as the strength of the electron donor increases.[29] As the electron-donating strength increases from carbazole to *N*,*N*-dimethylaniline, the absorption maximum shifts from 436 nm in **CSS** to 516 nm in **DSS**. On the other hand, the absorption maximum of the molecules would be affected by the conjugated unit.[30] For instance, the absorption maximum red shifts from 478 nm in **DLS** to 516 nm in **DSS**, which results from the extension of the π-conjugated unit. All the D–A molecules give a low photoluminescence signal in solution. However, the microstructures precipitated from their solutions are good emitters. Fluorescence spectra of the compounds were recorded in the solid state as shown in Fig. 2b. Their fluorescence maximum wavelengths (λ_{em}) range from 558 to 662 nm with about 100–200 nm of stoke's shift (Table 1).

Self-assemblies of CLS, DSS and CSS

The D–A molecules **CLS**, **DSS** and **CSS** were self-assembled into well-ordered and stable nanosized superstructures by simple solution methods without employing any surfactant, catalyst, or template. The operation parameters such as temperature, concentration, and growth time remarkably affected the morphologies of the ICT compounds in different self-assembled systems, due to the interactions of hydrogen bonds and π–π stacking in different chemical environments.[31] The molecular structures of the isoxazolone-based ICT compounds are the main factors that influence the aggregation of structures.

The compound **CLS** could form ribbon-like architectures. The operation process might be described as follows. Refluxing **CLS** (3 mg) in 8 mL of acetic ether at 80 °C for 10 min resulted in a transparent orange solution. Cooling down the solution in the oil bath for 1 h afforded the precipitates. As shown by scanning electron microscopy (SEM) and transmission electron microscopy (TEM) observations (see Fig. 3a and b), the precipitates were long micro-ribbons with the width of about 1 μm. These superstructures were so stable that they could preserve the ribbon-like morphology in acetic ether for weeks and even surmount ultrasonic concussion.

With the addition of ethanol, the compound **CSS** could be assembled into plate-like architectures through the solvent exchange method.[32] Injection of 0.3 mL CH_2Cl_2 solution of **CSS** into 2 mL well-stirred ethanol afforded orange precipitates. Washed with ethanol, the precipitates were immediately collected on the silicon grid. Fig. 3d and e show the typical morphologies of **CSS** microstructures. Large-scale plate-like architectures were observed in the SEM images. As shown in the TEM images, the plates are rhombic with a length of 40 μm and a width of about 10 μm.

Fig. 3c and f show the fluorescence microscopic images of the morphologies and fluorescence emission of the superstructures, which clearly confirm that the microstructures of **CLS** and **CSS** molecules are intense emitters. As mentioned in the crystal structure, the CH–π interactions extend over the whole crystal structure and the multiple intermolecular interactions help lock the molecular conformations. This kind of molecular configuration can effectively promote the π–π interaction in the solid state and has caused the intense fluorescence in the aggregated state.

The compound **DSS** would form hollow spheres or plate-like architectures under different operation conditions. **DSS** had good solubility in tetrahydrofuran, dichloromethane and acetone. But the solubility of **DSS** was poor in conventional organic solvents like hexane, methanol, ethanol, *etc.* Thus, slow

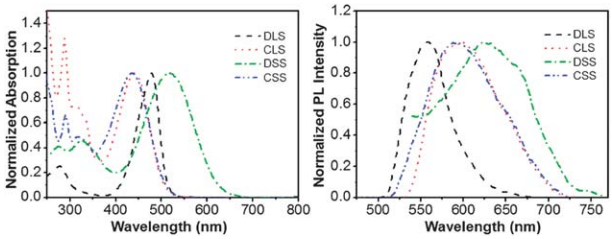

Fig. 2 Normalized optical absorption spectra of the donor–acceptor molecules in a dilute (1×10^{-5} M) CH_2Cl_2 solution (a). Normalized PL emission spectra in solid (b). The excitation wavelength used was 405 nm in all cases.

Table 1 Photophysical properties of four D–A molecules

Compd	λ_{abs}[a] (nm) (log ε)	λ_{em}[b] (nm)	Stoke's shift (nm)
DLS	277 (4.16), 478 (4.76)	558	80
CLS	288 (4.52), 308 (4.28), 441 (4.42)	600	159
DSS	275 (4.16), 326 (4.20), 516 (4.55)	624	108
CSS	290 (4.41), 321 (4.28), 436 (4.59)	592	156

[a] Measured in 1×10^{-5} M CH_2Cl_2 solution. [b] Measured in the solid.

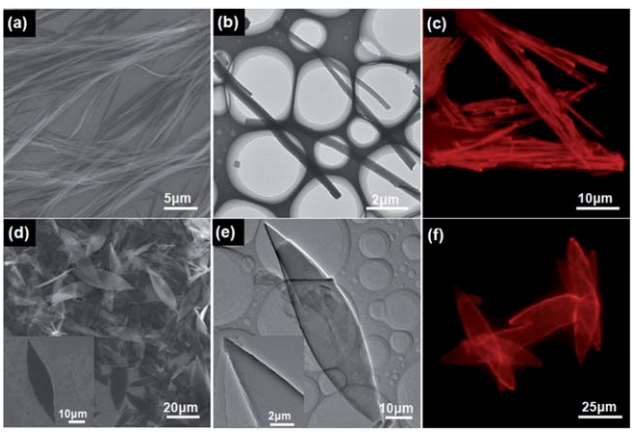

Fig. 3 Large-area SEM and TEM images of micro-ribbons of **CLS** (a and b). SEM and TEM images of **CSS** (d and e). Fluorescence microscopic images of **CLS** (c) and **CSS** (f) excited with a UV band (330–380 nm) light source.

crystallization was conducted at the interface between a "good" and a "poor" solvent. Well-defined hollow nanosphere structures of **DSS** were successfully fabricated by a phase transfer methodology.[33] The operation process of sphere architectures might be described as follows. At room temperature, 9 mL chromatographic grade hexane was added to the solution (1 mL with 3 mg DSS) very slowly. The system was kept undisturbed for a week and the nanostructures were afforded as the brown precipitates. The SEM and TEM observations of the precipitates are shown in Fig. 4a and b. The spheres with a diameter of 0.4–0.6 μm are observed. Interestingly, the images of SEM and TEM show that most of the spheres are hollow.

Beyond the solution processing method, a solvent-vapor technique[34] has been successfully used to obtain plate-like architectures on substrates. The operation process was described as follows. CH_2Cl_2 solution of **DSS** (1.14×10^{-3} M) was injected into the same volume solvent C_2H_5OH with sufficient stirring and a drop of the mixture was dropped onto the Si-waters directly. After the evaporation of the solvent, the nanostructure was obtained. This approach provides *in situ* preparation of microplates on a surface which are suitable for further optical or microscopy investigation and is not affected by the substrates. The SEM images (Fig. 4d) and TEM images (Fig. 4e) exhibit that the microstructures of DSS possess good plate-forming structures with a size of about 2 μm. The X-ray diffraction (XRD) pattern was taken to characterize the plate-like superstructures, as shown in the inset of Fig. 4e. The sharp diffraction peaks and the flat baseline in the XRD curves definitely demonstrate the perfect single-crystalline character of the architecture.[35] Six distinct peaks corresponding to the (006), (008), (113), (117), (122), (221) planes are clearly exhibited in the diffraction profile, which indicate that the preferred growth directions of the plate-like architectures are *a* axis and *b* axis and the preferred plane is the (001) plane. The thin plate morphology of DSS was also studied by atomic force microscopy (AFM), as shown in Fig. 4g and h. From the AFM images, we can observe that the surface of the platelike microstructures is pretty smooth. And it is interesting to note that the plates are multilayered in which the thickness of each layer is about 3.5 nm (shown in Fig. 4i). According to the distance of the π-stacking in the crystal structure of **DSS**, we could evaluate that each layer possesses about ten molecules. The formation of the microplates is driven by the combination of van der Waals interactions, π-stacking and hydrogen bonding. As shown in Fig. 1d, the isoxazolone acceptor units are responsible for the H-bonding interactions and the benzene ring in the donor units is responsible for the π-stacking interactions.

Fluorescence microscopic images were taken to examine the morphologies and fluorescence emission of hollow spheres and plate-like architectures of **DSS**, as shown in Fig. 4c and f, which indicate that **DSS** is a good red emitter.

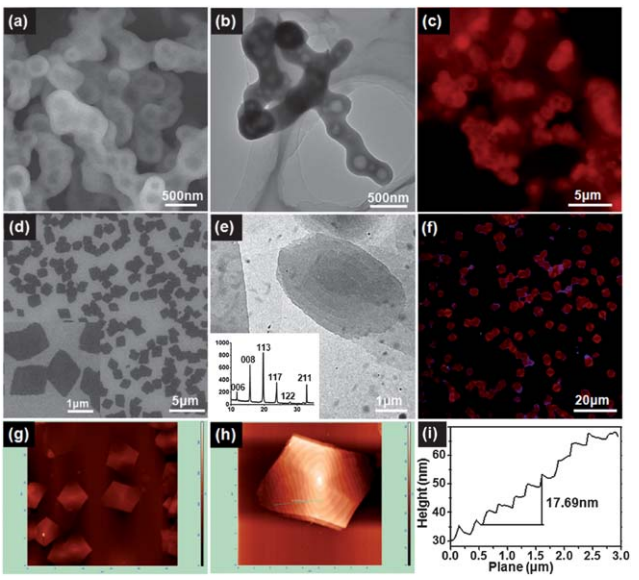

Fig. 4 SEM and TEM images of self-assembled hollow sphere (a and b) and plate-like (c and d) superstructures of **DSS**. The corresponding XRD pattern of plate-like aggregate structures (inset d). Fluorescence microscopic images of hollow sphere (c) and plate-like (f) superstructures of **DSS** excited with WIG green light source. AFM images (g and h) and the height phase (i) of self-assembled platelike superstructures of **DSS**.

Nonlinear optical properties

The third-order optical nonlinearities of all the compounds in CH_2Cl_2 were investigated by the *Z*-scan technique. This technique provided direct measurement of nonlinear absorption and refraction properties. The experimental process was similar to that in the literature.[36]

Nonlinear absorption effects of the compounds were evaluated under an open-aperture configuration. Fig. 5a shows the nonlinear absorptive curve of **CLS** in CH_2Cl_2. The filled squares represent the experimental data measured under the conditions. It is obvious that the absorption increases along with the increasing irradiance of the incident light. **CLS** exhibits a reverse saturated absorption behavior with the normalized power transmittance decreased at the focus by about 0.75 times compared to that of the low power transmittance. The solid line in Fig. 5a is the theoretical fitting curve from eqn (1).[37]

$$T(z) = \frac{1}{\sqrt{\pi}q(z)} \int_{-\infty}^{+\infty} \ln[1 + q(z)]e^{-\tau^2} d\tau$$
$$q(z) = \beta^{\text{eff}} I(z) \frac{1 - e^{-\alpha L}}{\alpha} \quad (1)$$

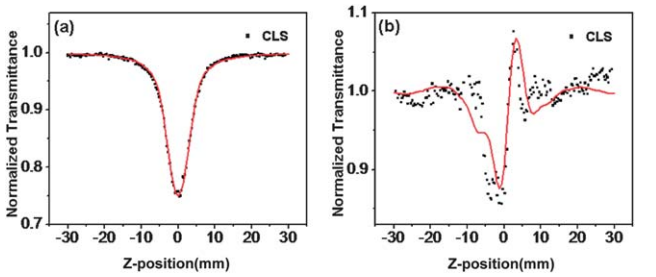

Fig. 5 Normalized open-aperture *Z*-scan curve (a) and closed-aperture *Z*-scan curve (b) of **CLS**. The solid lines are the fitting curves.

where α and β are linear and effective third-order NLO absorptive coefficients, τ is the time, and L is the sample length. Light transmittance (T) is a function of the sample's Z position (with respect to the focal point at $Z = 0$). A reasonably good fit between the experimental data and theoretical curve was obtained, which suggests that the experimentally obtained NLO effects are effectively third order in nature.[37] Thus, once an open-aperture Z-scan is performed, the nonlinear absorption coefficient β can be unambiguously deduced. Such as, the obtained nonlinear absorption coefficient β of **CLS** fitting the experimental data is 1.2×10^{-11} m W^{-1}. **DLS** and **CSS** show weaker coefficients, β, of 8.0×10^{-12} and 3.0×10^{-12} m W^{-1}, respectively (shown in Fig. S1†). On the other hand, the nonlinear refractive properties of the compounds were assessed by dividing the normalized Z-scan data obtained under the closed-aperture configuration by the normalized Z-scan data obtained under the open-aperture configuration. Fig. 5b shows the nonlinear refractive curve of **CLS** in CH_2Cl_2, and the valley followed by a peak indicates that the sign of the nonlinear refraction γ is positive *i.e.* self-focusing occurs. An effective third-order NLO refractive index γ can be obtained from the difference between normalized transmittance values at the valley and peak positions (ΔT_{p-v}) by using eqn (2).[37]

$$\gamma^{\text{eff}} = \frac{\lambda\alpha}{0.812\pi I(1 - e^{-\alpha L})}\Delta T_{v-p} \quad (2)$$

where ΔT_{p-v} is the difference between normalized transmittance values at the valley and peak positions, I is the peak irradiation intensity at the focus, and λ is the wavelength of the laser. The effective third-order nonlinear refractive indices of **CLS** and **DSS** (Fig. S2†) are 2.5×10^{-19} and 5.2×10^{-19} m^2 W^{-1}, respectively. All the data suggest the delocalized π-electronic configuration and intrinsic polarizability in the molecules, thus the compounds could be good candidates for third-order NLO materials.

Conclusions

In conclusion, we have synthesized four donor–acceptor molecules and investigated their crystal structures, self-assembly behaviors, and optical properties. The D–A molecules are good emitters in the solid state, but give a low photoluminescence signal in solution. These ICT compounds with different donors and different conjugation could be self-assembled into different superstructures. Interestingly, the morphologies of the microstructures would be diverse like hollow nanospheres or multilayered plates by employing different operating methods. Furthermore, all the compounds showed remarkable nonlinear responses which indicated π-electron delocalization and polarizability in the molecules. These results support our goals in the design and synthesis of new attractive NLO materials.

Experimental

Materials

All commercial available chemical reagents were purchased from Alfa Aesar or Aldrich Chemicals and utilized without further purification. Column chromatography was performed on silica gel (size 200–300 mesh). 4-(9*H*-Carbazol-9-yl)benzaldehyde (**1b**),[38] 4-(bromomethyl)benzaldehyde (**2**),[39] 2-(4-(bromomethyl)phenyl)-5,5-dimethyl-1,3-dioxane (**3**)[40] and (4-(5,5-dimethyl-1,3-dioxan-2-yl)benzyl)phosphonic acid diethyl ester (**4**)[41] were prepared according to the literature methods.

(*Z*)-4-(4-(Dimethylamino)benzylidene)-3-phenylisoxazol-5(4*H*)-one (DLS). To a three-necked flask were added **1a** (92 mg, 0.62 mmol) and ethanol (10 mL). The flask was equipped with a condenser and filled with argon to remove the air. Once the compound was dissolved, 3-phenyl-5-isoxazolone (100 mg, 0.62 mmol) was then added. The solution was refluxed under argon with exclusion of light for 2 h and then cooled down to room temperature. The resulting red precipitate was filtered off, washed with ethanol, and dried. Yield: 91%; ^{1}H NMR ($CDCl_3$, 400 MHz): 8.39 (d, $J = 8.8$ Hz, 2H), 7.57 (m, 2H), 7.54 (m, 3H), 7.39 (s, 1H), 6.72 (d, $J = 9.2$ Hz, 2H), δ 3.16 (s, 6H); ^{13}C NMR ($CDCl_3$, 125 MHz): δ 170.63, 164.95, 154.55, 151.78, 138.08, 130.40, 129.09, 128.95, 124.07, 122.08, 111.78, 110.05, 40.20; HRMS (EI mode) (m/z): found (M) 292.1216; calcd for $C_{18}H_{16}N_2O_2$: 292.1212.

(*Z*)-4-(4-(9*H*-Carbazol-9-yl)benzylidene)-3-phenylisoxazol-5(4*H*)-one (CLS). This compound was prepared by a procedure similar to that of **DLS** except that **1b** (168 mg, 0.62 mmol) was used as the reactant instead of **1a**. The resulting orange precipitate was filtered off, washed with ethanol, and dried. Yield: 78%; ^{1}H NMR ($CDCl_3$, 400 MHz): δ 8.62 (d, $J = 8.4$ Hz, 2H), 8.12 (d, $J = 7.6$ Hz, 2H), 7.74 (d, $J = 8.8$ Hz, 2H), 7.64 (m, 6H), 7.57 (d, $J = 8.4$ Hz, 2H), 7.44 (t, $J = 7.8$ Hz, 2H), 7.34 (t, $J = 7.6$ Hz, 2H); ^{13}C NMR ($CDCl_3$, 100 MHz): δ 168.51, 164.18, 151.13, 143.13, 139.93, 136.15, 131.22, 130.60, 129.44, 128.84, 127.66, 126.59, 126.35, 124.13, 121.27, 120.64, 118.61, 110.20; HRMS (EI mode) (m/z): found (M) 414.1375; calcd for $C_{28}H_{18}N_2O_2$: 414.1368.

(*Z*)-4-(4-((*E*)-4-(Dimethylamino)styryl)benzylidene)-3-phenylisoxazol-5(4*H*)-one (DSS). To a three-necked flask were added **6a** (130 mg, 0.52 mmol) and ethanol (30 mL). The flask was equipped with a condenser and filled with argon to remove the air. Once the compound was dissolved, 3-phenyl-5-isoxazolone (100 mg, 0.62 mmol) was then added. The solution was refluxed under argon with exclusion of light for 2 h and then cooled down to room temperature. The resulting brown precipitate was filtered off, washed with ethanol, and dried. The crude product was purified by recrystallization from ethyl acetate to afford the compound **DSS** as a brown powder. Yield: 80%; ^{1}H NMR ($CDCl_3$, 400 MHz): 8.35 (d, $J = 8.4$ Hz, 2H), 7.60 (m, 7H), 7.57 (s, 1H), 7.47 (d, $J = 8.4$ Hz, 2H), 7.29 (s, 1H), 6.98 (d, $J = 6.8$ Hz, 1H), 6.79 (s, 2H), 3.04 (s, 6H); ^{13}C NMR ($CDCl_3$, 125 MHz): δ 168.83, 164.40, 151.94, 150.57, 144.81, 135.20, 133.74, 131.12, 130.94, 129.35, 128.94, 128.65, 128.45, 128.40, 127.89, 126.42, 125.70, 116.86, 40.63; HRMS (EI mode) (m/z): found (M) 394.1687; calcd for $C_{26}H_{22}N_2O_2$: 394.1681.

(*E*)-9-(4-(4-(5,5-Dimethyl-1,3-dioxan-2-yl)styryl)phenyl)-9*H*-carbazole (5b). To a stirred solution of diethyl 4-(5,5-dimethyl-1,3-dioxan-2-yl)benzylphosphonate (0.784 g, 2.4 mmol) and 4-(9*H*-carbazol-9-yl)benzaldehyde (0.62 g, 2.3 mmol) in the DMF (20 mL) was added potassium butan-1-olate (0.3 g) several

times. The reaction mixture was then stirred in the ice bath for 30 minutes. About 150 mL of water was added into the mixture and the resulting mixture was extracted with dichloromethane. The organic layer was collected, washed with water and dried over anhydrous $MgSO_4$. The crude product was purified using a column chromatography silica gel with CH_2Cl_2–petroleum (1 : 1) to afford **5b** as a light yellow solid. Yield: 72%; ^{1}H NMR ($CDCl_3$, 400 MHz): 8.15 (d, J = 8.4 Hz, 2H), 7.74 (d, J = 8.4 Hz, 2H), 7.56 (m, 6H), 7.44 (m, 4H), 7.30 (m, 4H), 5.43 (s, 1H), 3.80 (d, J = 10.8 Hz, 2H), 3.68 (d, J = 10.8 Hz, 2H), 1.33 (s, 3H), 0.83 (s, 3H); ^{13}C NMR ($CDCl_3$, 100 MHz): δ 141.08, 138.48, 137.94, 137.14, 136.66, 129.49, 128.29, 128.16, 127.41, 126.97, 126.89, 126.35, 123.78, 120.68, 120.38, 110.20, 101.77, 30.54, 23.43, 22.20; HRMS (EI mode) (m/z): found (M) 459.2206; calcd for $C_{32}H_{29}NO_2$: 459.2198.

(*E*)-4-(4-(9*H*-Carbazol-9-yl)styryl)benzaldehyde (6b). To a stirred solution of **5b** (600 mg, 1.3 mmol) in CH_2Cl_2 was added 2 mL CF_3COOH slowly. The reaction mixture was then stirred at room temperature for 3–4 h (TLC monitoring). The reaction solution was washed with saturated aqueous Na_2CO_3 and dried over anhydrous $MgSO_4$. The crude product was purified by column chromatography silica gel with CH_2Cl_2–petroleum (2 : 1) to afford **6b** as a light yellow solid. Yield: 80%; ^{1}H NMR ($CDCl_3$, 400 MHz): 10.03 (s, 1H), 8.16 (d, J = 8.0 Hz, 2H), 7.91 (d, J = 8.4 Hz, 2H), 7.78 (d, J = 8.4 Hz, 2H), 7.71 (d, J = 8.0 Hz, 2H), 7.61 (d, J = 8.4 Hz, 2H), 7.44 (m, 4H), 7.31 (m, 3H), 7.22 (s, 1H); ^{13}C NMR ($CDCl_3$, 100 MHz): δ 191.77, 143.34, 140.87, 137.93, 135.82, 135.73, 131.30, 130.51, 128.45, 128.34, 127.46, 127.23, 126.23, 123.73, 120.59, 120.36, 110.00; HRMS (EI mode) (m/z): found (M) 373.1472; calcd for $C_{27}H_{19}NO$: 373.1467.

(*Z*)-4-(4-((*E*)-4-(9*H*-Carbazol-9-yl)styryl)benzylidene)-3-phenylisoxazol-5(4*H*)-one (CSS). This compound was prepared by a procedure similar to that of **DSS** except that **6b** (194 mg, 0.52 mmol) was used as the reactant instead of **6a**. The resulting red precipitate was filtered off, washed with ethanol, and dried. The crude product was purified by recrystallization from CH_2Cl_2–petroleum to afford the compound **CSS** as a red powder. Yield: 86%; ^{1}H NMR ($CDCl_3$, 400 MHz): 8.40 (d, J = 8.4 Hz, 2H), 8.15 (d, J = 7.6 Hz, 2H), 7.79 (d, J = 8.4 Hz, 2H), 7.69 (d, J = 8.4 Hz, 2H), 7.61 (m, 8H), 7.40 (m, 6H), 7.31 (t, J = 6.8 Hz, 2H); ^{13}C NMR ($CDCl_3$, 125 MHz): δ 168.53, 164.25, 151.74, 143.18, 140.75, 138.05, 135.61, 134.99, 132.06, 131.90, 131.09, 129.42, 128.91, 128.50, 128.20, 127.66, 127.36, 127.09, 126.15, 123.67, 120.50, 120.30, 118.10, 109.91; HRMS (EI mode) (m/z): found (M) 516.1843; calcd for $C_{36}H_{24}N_2O_2$: 516.1838.

Characterization

^{1}H and ^{13}C NMR spectra were recorded on a Bruker ARX400 spectrometer with tetramethylsilane (TMS) as the internal standard; chemical shifts (δ) are given in ppm relative to TMS. EI mass spectrometric measurements were obtained on the SHIMADZU GCMS-QP2010 pulse spectrometer. All single-crystal X-ray diffraction data were collected on a Rigaku Saturn X-ray diffractometer with graphite monochromator Mo Kα radiation (λ = 0.71073 Å) at 173 K. Intensities were collected for absorption effects using the multiscan technique SADABS. The structures were solved by direction methods and refined by a full-matrix least-squares technique based on F2 using the SHELXL 97 program (Sheldrick, 1997). The extended packing plots and data from crystal packing were obtained using the software Mercury 1.4.1 and ORTEP 3.

UV-vis absorption spectra were recorded on a Hitachi U-3100 spectrometer. Fluorescence spectra and images of the microstructures were taken by using a laser-based fluorescence microscope (Olympus IX81). SEM images were taken using a Hitachi S-4800 microscope at an accelerating voltage of 10 kV or 15 kV. TEM images were taken using a JEOL JEM-1011 microscope at an accelerating voltage of 100 kV. The assemblies were also characterized by X-ray diffraction (XRD, Japan Rigaku D/max-2500) with Cu Kα radiation at a rate of three degree per minute. AFM measurements were carried out by the NT-MDT.

Nonlinear absorption was measured by using the open-aperture *Z*-scan. A Q-switched laser was used as the light source, which provided linearly polarized 4 ns with a repetition rate of 2 Hz at 532 nm. The spatial profiles of optical pulses were nearly Gaussian obtained by spatial filtering. The samples were placed in quartz cells with 2 mm thickness, which were placed at the focus of a lens with a focal length of 60 cm. The laser pulses adjusted by an attenuator were separated into beams by using a splitter. The two beams were simultaneously measured by using two energy detectors (818J-09B energy probe, Newport Corporation) linked to the energy meter (model 2835-C, Newport). A personal computer was used to collect the data coming from the energy meter through the RS-232C interface.

Acknowledgements

This work was supported by the National Nature Science Foundation of China (50825202, 51072064, 21031006) and the National Basic Research 973 Program of China (2009CB939701, 2011CB935800, 2011CB932302, 2012CB932900).

Notes and references

1 A. Apostoluk, J.-M. Nunzi, I. F. Perepichka, Z. V. Stepanenko and I. M. Serebryakov, *Chem. Phys.*, 2007, **331**, 339–345.
2 T. Michinobu, J. C. May, J. H. Lim, C. Boudon, J.-P. Gisselbrecht, P. Seiler, M. Gross, I. Biaggio and F. Diederich, *Chem. Commun.*, 2005, 737–739.
3 T. Michinobu, C. Boudon, J.-P. Gisselbrecht, P. Seiler, B. Frank, N. N. P. Moonen, M. Gross and F. Diederich, *Chem.–Eur. J.*, 2006, **12**, 1889–1905.
4 O.-K. Kim, K.-S. Lee, H. Y. Woo, K.-S. Kim, G. S. He, J. Swiatkiewicz and P. N. Prasad, *Chem. Mater.*, 2000, **12**, 284–286.
5 S. Chen, Y. Li, W. Yang, N. Chen, H. Liu and Y. Li, *J. Phys. Chem. C*, 2010, **114**, 15109–15115.
6 M. Kivala and F. o. Diederich, *Acc. Chem. Res.*, 2008, **42**, 235–248.
7 J. Xu, L. Wen, W. Zhou, J. Lv, Y. Guo, M. Zhu, H. Liu, Y. Li and L. Jiang, *J. Phys. Chem. C*, 2009, **113**, 5924–5932.
8 J. Xu, S. Semin, D. Niedzialek, P. H. J. Kouwer, E. Fron, E. Coutino, M. Savoini, Y. Li, J. Hofkens, H. Uji-I,

D. Beljonne, T. Rasing and A. E. Rowan, *Adv. Mater.*, 2013, **25**, 2084–2089.
9 L. Beverina, J. Fu, A. Leclercq, E. Zojer, P. Pacher, S. Barlow, E. W. Van Stryland, D. J. Hagan, J.-L. Brédas and S. R. Marder, *J. Am. Chem. Soc.*, 2005, **127**, 7282–7283.
10 A. Abbotto, L. Beverina, R. Bozio, A. Facchetti, C. Ferrante, G. A. Pagani, D. Pedron and R. Signorini, *Chem. Commun.*, 2003, 2144–2145.
11 R. Y. Lai, X. Kong, S. A. Jenekhe and A. J. Bard, *J. Am. Chem. Soc.*, 2003, **125**, 12631–12639.
12 A. P. Kulkarni, X. Kong and S. A. Jenekhe, *Adv. Funct. Mater.*, 2006, **16**, 1057–1066.
13 X. Jiang, X. Yang, C. Zhao, K. Jin and L. Sun, *J. Phys. Chem. C*, 2007, **111**, 9595–9602.
14 A. W. Czarnik, *Acc. Chem. Res.*, 1994, **27**, 302–308.
15 T.-D. Kim, J.-W. Kang, J. Luo, S.-H. Jang, J.-W. Ka, N. Tucker, J. B. Benedict, L. R. Dalton, T. Gray, R. M. Overney, D. H. Park, W. N. Herman and A. K. Y. Jen, *J. Am. Chem. Soc.*, 2007, **129**, 488–489.
16 S. E.-D. H. Etaiw, T. A. Fayed and N. Z. Saleh, *J. Photochem. Photobiol., A*, 2006, **177**, 238–247.
17 P. Dutta, J. Kim, S. H. Eom, W.-H. Lee, I. N. Kang and S.-H. Lee, *ACS Appl. Mater. Interfaces*, 2012, **4**, 6669–6675.
18 S. Steinberger, A. Mishra, E. Reinold, C. M. Müller, C. Uhrich, M. Pfeiffer and P. Bäuerle, *Org. Lett.*, 2010, **13**, 90–93.
19 L.-Y. Lin, C.-W. Lu, W.-C. Huang, Y.-H. Chen, H.-W. Lin and K.-T. Wong, *Org. Lett.*, 2011, **13**, 4962–4965.
20 J. L. Bredas, C. Adant, P. Tackx, A. Persoons and B. M. Pierce, *Chem. Rev.*, 1994, **94**, 243–278.
21 H. S. Nalwa, *Adv. Mater.*, 1993, **5**, 341–358.
22 S. Alías, R. Andreu, M. a. J. s. Blesa, M. A. Cerdán, S. Franco, J. Garín, C. López, J. s. Orduna, J. Sanz, R. Alicante, B. n. Villacampa and M. Allain, *J. Org. Chem.*, 2008, **73**, 5890–5898.
23 J. Hua, J. Luo, J. Qin, Y. Shen, Y. Zhang and Z. Lu, *J. Mater. Chem.*, 2002, **12**, 863–867.
24 W. Gong, Q. Li, Z. Li, C. Lu, J. Zhu, S. Li, J. Yang, Y. Cui and J. Qin, *J. Phys. Chem. B*, 2006, **110**, 10241–10247.
25 M. Mirzazadeh and G. H. Mahdavinia, *Chem.–Eur. J*, 2012, **9**, 425–429.
26 J.-Z. Zhao, F.-L. Liu, H.-B. Song, X.-F. Liu and Z.-J. Fan, *Acta Crystallogr., Sect. E: Struct. Rep. Online*, 2006, **62**, o630–o631.
27 L. Li, Y. Wu, Q. Zhou and C. He, *J. Phys. Org. Chem.*, 2012, **25**, 362–372.
28 J. M. Hancock, A. P. Gifford, Y. Zhu, Y. Lou and S. A. Jenekhe, *Chem. Mater.*, 2006, **18**, 4924–4932.
29 Y. Zhu, A. P. Kulkarni, P.-T. Wu and S. A. Jenekhe, *Chem. Mater.*, 2008, **20**, 4200–4211.
30 K.-F. Chen, Y.-C. Hsu, Q. Wu, M.-C. P. Yeh and S.-S. Sun, *Org. Lett.*, 2008, **11**, 377–380.
31 S. H. Chen, N. Chen, Y. L. Yan, T. F. Liu, Y. W. Yu, Y. J. Li, H. B. Liu, Y. S. Zhao and Y. L. Li, *Chem. Commun.*, 2012, **48**, 9011–9013.
32 J. Xu, X. Liu, J. Lv, M. Zhu, C. Huang, W. Zhou, X. Yin, H. Liu, Y. Li and J. Ye, *Langmuir*, 2008, **24**, 4231–4237.
33 K. Balakrishnan, A. Datar, T. Naddo, J. Huang, R. Oitker, M. Yen, J. Zhao and L. Zang, *J. Am. Chem. Soc.*, 2006, **128**, 7390–7398.
34 R. van Hameren, P. Schön, A. M. van Buul, J. Hoogboom, S. V. Lazarenko, J. W. Gerritsen, H. Engelkamp, P. C. M. Christianen, H. A. Heus, J. C. Maan, T. Rasing, S. Speller, A. E. Rowan, J. A. A. W. Elemans and R. J. M. Nolte, *Science*, 2006, **314**, 1433–1436.
35 J. Xu, H. Zheng, H. Liu, C. Zhou, Y. Zhao, Y. Li and Y. Li, *J. Phys. Chem. C*, 2010, **114**, 2925–2931.
36 H. Sakurai, M. T. S. Ritonga, H. Shibatani and T. Hirao, *J. Org. Chem.*, 2005, **70**, 2754–2762.
37 C. Zhang, Y. L. Song, Y. Xu, H. Fun, G. Y. Fang, Y. X. Wang and X. Q. Xin, *J. Chem. Soc., Dalton Trans.*, 2000, 2823–2829.
38 B. Hu, F. Zhuge, X. Zhu, S. Peng, X. Chen, L. Pan, Q. Yan and R.-W. Li, *J. Mater. Chem.*, 2012, **22**, 520–526.
39 Y. Endo, M. Ohno, M. Hirano, A. Itai and K. Shudo, *J. Am. Chem. Soc.*, 1996, **118**, 1841–1855.
40 P. Mateus, R. Delgado, P. Groves, S. R. R. Campos, A. M. Baptista, P. Brandão and V. Félix, *J. Org. Chem.*, 2012, **77**, 6816–6824.
41 G. Accorsi, N. Armaroli, J.-F. Eckert and J.-F. Nierengarten, *Tetrahedron Lett.*, 2002, **43**, 65–68.

